Chapter 6
The Double Pendulum

6.1 HAMILTON's Equations

We investigate the dynamics of the double pendulum in two spacial dimensions as illustrated schematically in Fig. 6.1. It is the aim of this section to derive HAMILTON's equations of motion for this system. In a first step we introduce generalized coordinates and determine the LAGRANGE function of the system from its kinetic and potential energy [1–5]. We then introduce generalized momenta and, finally, derive the HAMILTON function from which HAMILTON's equations of motion follow. They will serve as a starting point for the formulation of a numerical method.

From Fig. 6.1 we find the coordinates of the two point masses m:

$$x_1 = \ell \sin(\varphi_1) \ , \qquad z_1 = 2\ell - \ell \cos(\varphi_1) \ , \tag{6.1}$$

and

$$x_2 = \ell \left[\sin(\varphi_1) + \sin(\varphi_2)\right] \ , \qquad z_2 = 2\ell - \ell \left[\cos(\varphi_1) + \cos(\varphi_2)\right] \ . \tag{6.2}$$

Here, 2ℓ is the pendulum's total length. The angles φ_i, $i = 1, 2$ are defined in Fig. 6.1.

We note that $\ell = \text{const}$ and obtain the time derivatives of the coordinates (6.1) and (6.2):

$$\dot{x}_1 = \ell \dot{\varphi}_1 \cos(\varphi_1) \ , \tag{6.3}$$

$$\dot{z}_1 = \ell \dot{\varphi}_1 \sin(\varphi_1) \ , \tag{6.4}$$

$$\dot{x}_2 = \ell \left[\dot{\varphi}_1 \cos(\varphi_1) + \dot{\varphi}_2 \cos(\varphi_2)\right] \ , \tag{6.5}$$

$$\dot{z}_2 = \ell \left[\dot{\varphi}_1 \sin(\varphi_1) + \dot{\varphi}_2 \sin(\varphi_2)\right] \ . \tag{6.6}$$

B.A. Stickler, E. Schachinger, *Basic Concepts in Computational Physics*,
DOI 10.1007/978-3-319-27265-8_6

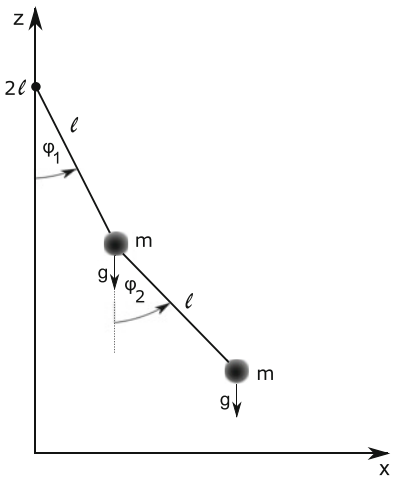

Fig. 6.1 Schematic illustration of the double pendulum. m are the point-masses, 2ℓ is the total length of the pendulum and φ_1, φ_2 are the corresponding angles

The LAGRANGE function of the system is defined by

$$L = T - U \,, \tag{6.7}$$

with the kinetic energy T and the potential U. The kinetic energy T is given by[1]

$$\begin{aligned} T &= \frac{m}{2}\left(\dot{x}_1^2 + \dot{z}_1^2 + \dot{x}_2^2 + \dot{z}_2^2\right) \\ &= \frac{m\ell^2}{2}\left[2\dot{\varphi}_1^2 + \dot{\varphi}_2^2 + 2\dot{\varphi}_1\dot{\varphi}_2\cos(\varphi_1 - \varphi_2)\right] \,. \end{aligned} \tag{6.8}$$

The potential energy U is determined by the gravitational force

$$\begin{aligned} U &= mgz_1 + mgz_2 \\ &= mg\ell\left[4 - 2\cos(\varphi_1) - \cos(\varphi_2)\right] \,, \end{aligned} \tag{6.9}$$

where g is the acceleration due to gravity. Hence, we get for the LAGRANGE function L:

$$L = \frac{m\ell^2}{2}\left[2\dot{\varphi}_1^2 + \dot{\varphi}_2^2 + 2\dot{\varphi}_1\dot{\varphi}_2\cos(\varphi_1 - \varphi_2)\right] - mg\ell\left[4 - 2\cos(\varphi_1) - \cos(\varphi_2)\right] \,. \tag{6.10}$$

[1] We make use of the relation:

$$\sin(x)\sin(y) + \cos(x)\cos(y) = \cos(x - y) \,.$$

We find a description of the motion in phase space by calculating the generalized momenta p_i, $i = 1, 2$ as

$$p_1 = \frac{\partial}{\partial \dot{\varphi}_1} L = m\ell^2 \left[2\dot{\varphi}_1 + \dot{\varphi}_2 \cos(\varphi_1 - \varphi_2)\right] , \tag{6.11}$$

and

$$p_2 = \frac{\partial}{\partial \dot{\varphi}_2} L = m\ell^2 \left[\dot{\varphi}_2 + \dot{\varphi}_1 \cos(\varphi_1 - \varphi_2)\right] . \tag{6.12}$$

The aim is now to express the kinetic energy (6.8) in terms of generalized momenta p_1 and p_2. To accomplish this we solve in a first step Eq. (6.12) for $\dot{\varphi}_2$ and obtain

$$\dot{\varphi}_2 = \frac{p_2}{m\ell^2} - \dot{\varphi}_1 \cos(\varphi_1 - \varphi_2) . \tag{6.13}$$

This is used to rewrite Eq. (6.11). Solving for $\dot{\varphi}_1$ gives:

$$\dot{\varphi}_1 = \left[2 - \cos^2(\varphi_1 - \varphi_2)\right]^{-1} \left[\frac{p_1}{m\ell^2} - \frac{p_2}{m\ell^2} \cos(\varphi_1 - \varphi_2)\right] . \tag{6.14}$$

The trigonometric identity $\cos^2(x) + \sin^2(x) = 1$ changes Eq. (6.14) into

$$\dot{\varphi}_1 = \frac{1}{m\ell^2} \frac{p_1 - p_2 \cos(\varphi_1 - \varphi_2)}{1 + \sin^2(\varphi_1 - \varphi_2)} . \tag{6.15}$$

This is then used to transform Eq. (6.13) into

$$\begin{aligned} \dot{\varphi}_2 &= \frac{1}{m\ell^2} \left[p_2 - \frac{p_1 \cos(\varphi_1 - \varphi_2) - p_2 \cos^2(\varphi_1 - \varphi_2)}{1 + \sin^2(\varphi_1 - \varphi_2)}\right] \\ &= \frac{1}{m\ell^2} \frac{2p_2 - p_1 \cos(\varphi_1 - \varphi_2)}{1 + \sin^2(\varphi_1 - \varphi_2)} . \end{aligned} \tag{6.16}$$

Hence, with help of Eqs. (6.15) and (6.16) we can reevaluate the kinetic energy (6.8) to give

$$\begin{aligned} T &= \frac{m\ell^2}{2} \left[2\dot{\varphi}_1^2 + \dot{\varphi}_2^2 + 2\dot{\varphi}_1 \dot{\varphi}_2 \cos(\varphi_1 - \varphi_2)\right] \\ &= \frac{1}{2m\ell^2} \frac{p_1^2 + 2p_2^2 - 2p_1 p_2 \cos(\varphi_1 - \varphi_2)}{1 + \sin^2(\varphi_1 - \varphi_2)} . \end{aligned} \tag{6.17}$$

The HAMILTON function $H(p_1, p_2, \varphi_1, \varphi_2)$ is the sum of the kinetic energy (6.17) and the potential energy (6.9) and we get:

$$\begin{aligned} H &= T + U \\ &= \frac{1}{2m\ell^2} \frac{p_1^2 + 2p_2^2 - 2p_1 p_2 \cos(\varphi_1 - \varphi_2)}{1 + \sin^2(\varphi_1 - \varphi_2)} \\ &\quad + mg\ell \left[4 - 2\cos(\varphi_1) - \cos(\varphi_2)\right] . \end{aligned} \tag{6.18}$$

Thus, we are now, finally, in a position to formulate HAMILTON's equations of motion from

$$\dot{\varphi}_i = \frac{\partial}{\partial p_i} H , \quad \dot{p}_i = -\frac{\partial}{\partial \varphi_i} H , \quad i = 1, 2, \tag{6.19}$$

and the dynamics of the double pendulum are determined by the solutions of the following set of differential equations:

$$\dot{\varphi}_1 = \frac{1}{m\ell^2} \frac{p_1 - p_2 \cos(\varphi_1 - \varphi_2)}{1 + \sin^2(\varphi_1 - \varphi_2)} , \tag{6.20a}$$

$$\dot{\varphi}_2 = \frac{1}{m\ell^2} \frac{2p_2 - p_1 \cos(\varphi_1 - \varphi_2)}{1 + \sin^2(\varphi_1 - \varphi_2)} , \tag{6.20b}$$

$$\begin{aligned} \dot{p}_1 = \frac{1}{m\ell^2} \frac{1}{1 + \sin^2(\varphi_1 - \varphi_2)} \Bigg[& -p_1 p_2 \sin(\varphi_1 - \varphi_2) \\ & + \frac{p_1^2 + 2p_2^2 - 2p_1 p_2 \cos(\varphi_1 - \varphi_2)}{1 + \sin^2(\varphi_1 - \varphi_2)} \cos(\varphi_1 - \varphi_2) \sin(\varphi_1 - \varphi_2) \Bigg] \\ & - 2mg\ell \sin(\varphi_1) , \end{aligned} \tag{6.20c}$$

and

$$\begin{aligned} \dot{p}_2 = \frac{1}{m\ell^2} \frac{1}{1 + \sin^2(\varphi_1 - \varphi_2)} \Bigg[& p_1 p_2 \sin(\varphi_1 - \varphi_2) \\ & - \frac{p_1^2 + 2p_2^2 - 2p_1 p_2 \cos(\varphi_1 - \varphi_2)}{1 + \sin^2(\varphi_1 - \varphi_2)} \sin(\varphi_1 - \varphi_2) \cos(\varphi_1 - \varphi_2) \Bigg] \\ & - mg\ell \sin(\varphi_2) . \end{aligned} \tag{6.20d}$$

The following section is dedicated to the numerical solution of Eqs. (6.20) with the help of the explicit RUNGE-KUTTA algorithm *e-RK-4* introduced in Sect. 5.3.

6.2 Numerical Solution

In a first step we recognize that Eqs. (6.20) are of the form

$$\dot{y} = F(y) \,, \tag{6.21}$$

where $y \in \mathbb{R}^4$. Let us define

$$y = \begin{pmatrix} y_1 \\ y_2 \\ y_3 \\ y_4 \end{pmatrix} \equiv \begin{pmatrix} \varphi_1 \\ \varphi_2 \\ p_1 \\ p_2 \end{pmatrix} \,, \tag{6.22}$$

and consequently

$$\begin{pmatrix} \dot{\varphi}_1 \\ \dot{\varphi}_2 \\ \dot{p}_1 \\ \dot{p}_2 \end{pmatrix} = F(y) \equiv \begin{pmatrix} f_1(y) \\ f_2(y) \\ f_3(y) \\ f_4(y) \end{pmatrix} \,. \tag{6.23}$$

We introduce time instances $t_n = n\Delta t$, $n \in \mathbb{N}$ and use the notation $y_n \equiv y(t_n) = (y_1^n, y_2^n, y_3^n, y_4^n)^T$. Furthermore, $F(y)$ is not an explicit function of time t and we reformulate the *e-RK-4* algorithm of Eq. (5.39) as:

$$\begin{aligned} Y_1 &= y_n \,, \\ Y_2 &= y_n + \frac{\Delta t}{2} F(Y_1) \,, \\ Y_3 &= y_n + \frac{\Delta t}{2} F(Y_2) \,, \\ Y_4 &= y_n + \Delta t F(Y_3) \,, \\ y_{n+1} &= y_n + \frac{\Delta t}{6} \left[F(Y_1) + 2F(Y_2) + 2F(Y_3) + F(Y_4) \right] \,. \end{aligned} \tag{6.24}$$

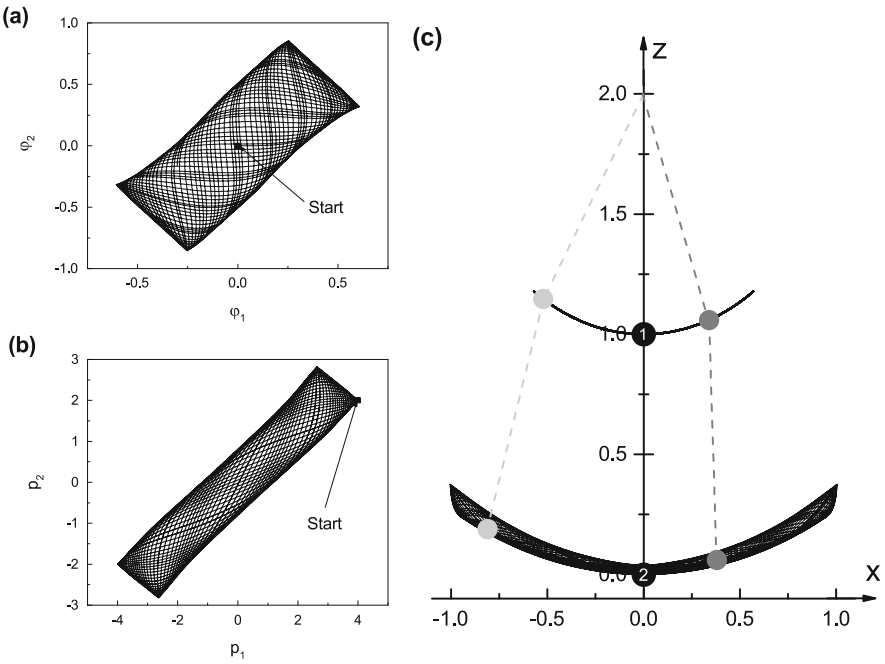

Fig. 6.2 Numerical solution of the double pendulum with initial conditions $\varphi_1(0) = \varphi_2(0) = 0.0$, $p_1(0) = 4.0$ and $p_2(0) = 2.0$. **(a)** Trajectory in φ-space, **(b)** trajectory in p-space, and **(c)** trajectory in local (x, z)-space. The *solid circles* numbered 1 and 2 represent the two masses in their initial configuration

Hence, the only remaining challenge is to correctly implement the function $F(y) = [f_1(y), f_2(y), f_3(y), f_4(y)]^T$ according to Eqs. (6.20).

The following graphs discuss the dynamics (trajectories in φ- and p-space, as well as in configuration space) of the pendulum and for this purpose we defined the parameters $m = \ell = 1$ and $g = 9.8067$. The time step was chosen to be $\Delta t = 0.001$ and we calculated $N = 60{,}000$ time steps.

We start with Fig. 6.2. The two masses numbered 1 and 2 are initially in the equilibrium position (solid circles). Both masses are pushed to the right but the push on mass 1 $[p_1(0) = 4.0]$ is much stronger than the one mass 2 experiences $[p_2(0) = 2.0]$. Thus, mass 2 is 'dragged' along in the process. This is made transparent by two 'snapshots' indicated by solid light gray circles and solid gray circles. The motion of the whole system is quite regular.

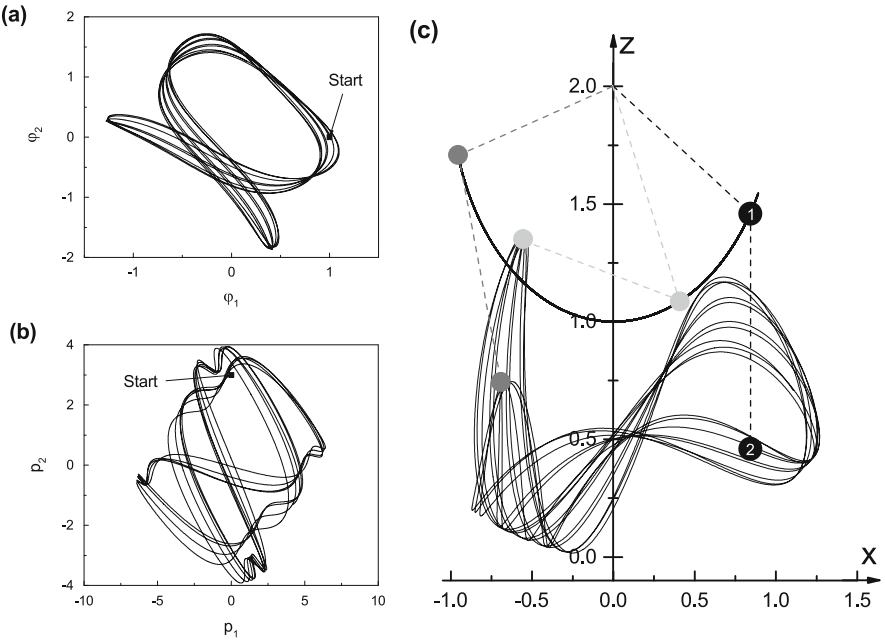

Fig. 6.3 Numerical solution of the double pendulum with initial conditions $\varphi_1(0) = 1.0, \varphi_2(0) = 0.0, p_1(0) = 0.0$ and $p_2(0) = 3.0$. **(a)** Trajectory in φ-space, **(b)** trajectory in p-space, and **(c)** trajectory in local (x, z)-space. The *solid circles* numbered 1 and 2 represent the two masses in their initial configuration

We proceed with Fig. 6.3. In this case mass 1 is displaced from its position by the initial angular displacement $\varphi_1 = 1.0$. This initial configuration is indicated by the solid circles numbered 1 and 2 representing the two point-masses. Mass 2 is then pushed to the right with $p_2(0) = 3.0$. Again, mass 1 remains on a trajectory centered around the point (0,2) in configuration space. But in contrast to the previous situation it follows now mass 2. Mass 2, on the other hand, develops a very lively trajectory, Fig. 6.3c. Two snapshots indicated by solid light gray circles and solid gray circles illustrate configurations of particular interest.

The dynamics depicted in Fig. 6.4 is quite similar to the one already discussed in Fig. 6.2. Initially both masses are in the equilibrium position and then mass 2 is pushed to the right [$p_2(0) = 4.0$]. Thus, mass 1 is trailing behind. In contrast to the previous Fig. 6.3 the trajectory of mass 2 will now be symmetric around the z-axis given enough time. Again, snapshots indicated by solid light gray circles and solid gray circles indicate interesting configurations.

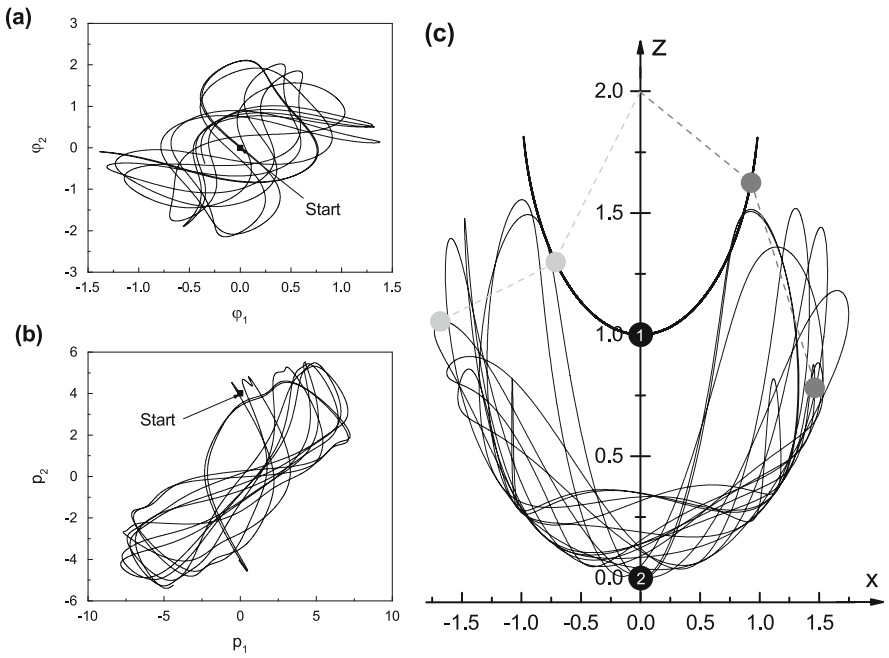

Fig. 6.4 Numerical solution of the double pendulum with initial conditions $\varphi_1(0) = \varphi_2(0) = 0.0$, $p_1(0) = 0.0$ and $p_2(0) = 4.0$. **(a)** Trajectory in φ-space, **(b)** trajectory in p-space, and **(c)** trajectory in local (x, z)-space. The *solid circles* numbered 1 and 2 represent the two masses in their initial configuration

The initial condition which resulted in the trajectory shown in Fig. 6.5 differs only for mass 2 from the initial conditions which lead to the trajectory in Fig. 6.4. Mass 2 is now pushed even more strongly to the right [$p_2(0) = 5.0$]. Of course, mass 1 is again dragging behind mass 2. In contrast to Fig. 6.4 the initial momentum of mass 2 is now sufficient to allow mass 2 to pass through the center of the inner mass' circular trajectory. Snapshots indicated by light gray solid circles and solid gray circles emphasize interesting configurations.

The situation shown in Fig. 6.6 differs from the one of Fig. 6.5 only by the initial condition for mass 2. It is now pushed even more strongly to the right [$p_2(0) = 6.5$] and this initial momentum is sufficient to cause mass 1 to rotate around the point (0,2). Nevertheless, mass 1 is permanently dragging behind mass 2. Two interesting configurations are depicted by snapshots (solid light gray circles and solid gray circles).

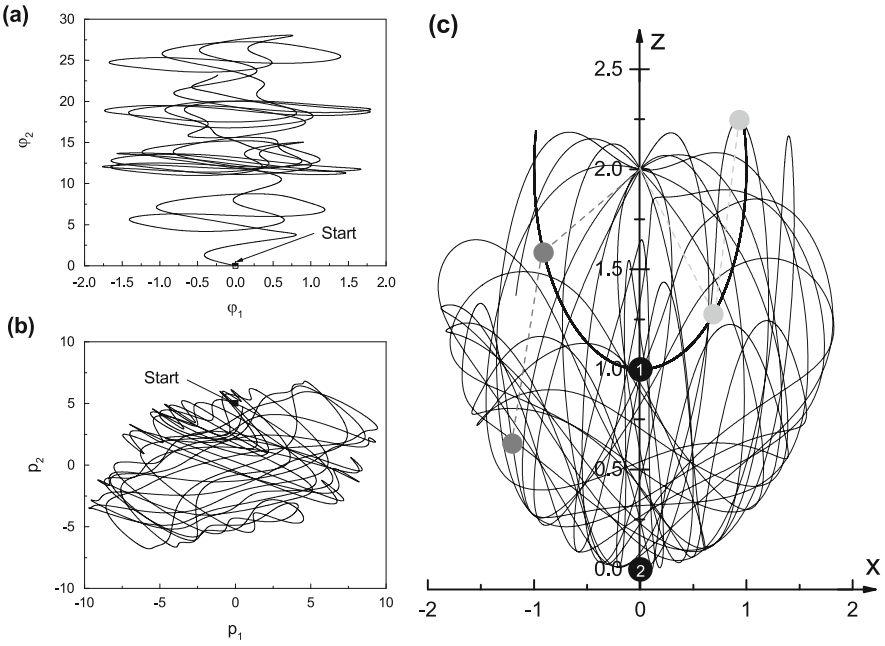

Fig. 6.5 Numerical solution of the double pendulum with initial conditions $\varphi_1(0) = \varphi_2(0) = 0.0$, $p_1(0) = 0.0$ and $p_2(0) = 5.0$. **(a)** Trajectory in φ-space, **(b)** trajectory in p-space, and **(c)** trajectory in local (x, z)-space. The *solid circles* numbered 1 and 2 represent the two masses in their initial configuration (The angles $\varphi_2 > \pi$ correspond to complete rotations of the pendulum)

A comparison between trajectories as a result of different initial conditions reveals that the physical system is highly sensitive to the choice of the initial conditions $y_0 = [\varphi_1(0), \varphi_2(0), p_1(0), p_2(0)]^T$. For instance, consider Figs. 6.4, 6.5, and 6.6. In all three cases we chose y_0 in such a way that the initial angles $\varphi_1(0) = \varphi_2(0) = 0$ and the generalized momentum coordinate $p_1(0) = 0$. The only difference is that we used different values for the initial value of the second momentum coordinate p_2. However, the resulting dynamics of φ_1 vs. φ_2 as well as p_1 vs. p_2 are entirely different and so are the local (x, z)-space trajectories. Hence, the system is *chaotic*. In the following section we will briefly discuss a method designed to characterize chaotic behavior of physical systems [6–10].

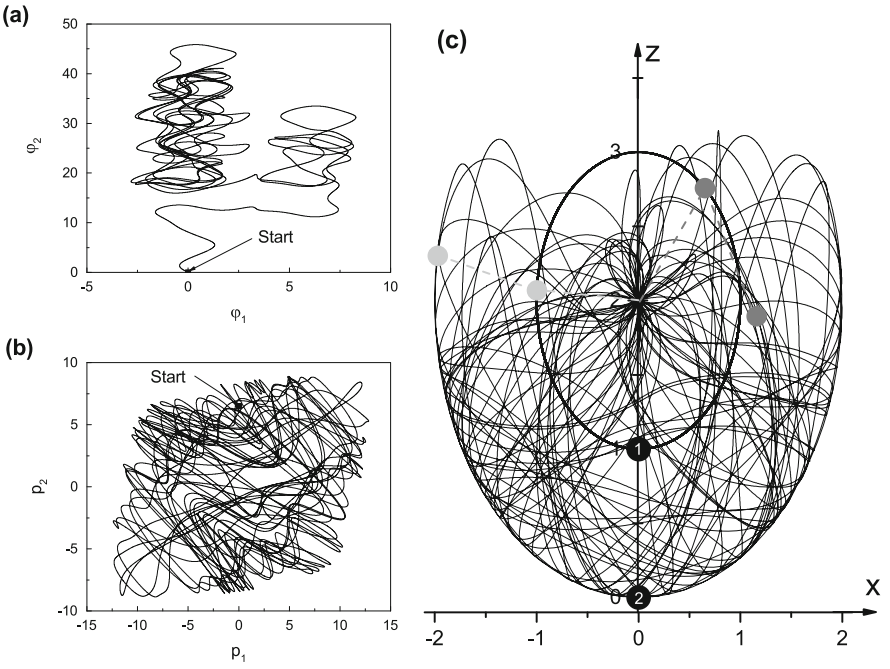

Fig. 6.6 Numerical solution of the double pendulum with initial conditions $\varphi_1(0) = \varphi_2(0) = 0.0$, $p_1(0) = 0.0$ and $p_2(0) = 6.5$. **(a)** Trajectory in φ-space, **(b)** trajectory in p-space, and **(c)** trajectory in configuration space. The *solid circles* numbered 1 and 2 represent the two masses in their initial configuration (The angles $\varphi_2 > \pi$ correspond to complete rotations of the pendulum)

6.3 Numerical Analysis of Chaos

It is the aim of this section to analyze in more detail the chaotic behavior observed in the dynamics of the double pendulum. This requires the introduction of some basic notations. We consider a physical system with f degrees of freedom where $q_1(t), \ldots, q_f(t)$ denote the generalized coordinates and $p_1(t), \ldots, p_f(t)$ denote the corresponding generalized momenta. Together, both fully characterize the state of the system at time t. Consequently, the f-dimensional vector $q(t) = [q_1(t), q_2(t), \ldots, q_f(t)]^T$ describes a point in *configuration space* of the physical system. In case of a pendulum consisting of f point-masses connected in a similar fashion as the double pendulum discussed above, which corresponds to the particular case $f = 2$, the configuration space is constrained to values $\varphi_i \in (-\pi, \pi]$, $i = 1, \ldots, f$. This resembles an f-dimensional torus.

The $2f$-dimensional vector $x(t) = [q_1(t), \ldots, q_f(t), p_1(t), \ldots, p_f(t)]^T$ describes a point in the *phase space* of the physical system at some particular time t. The

time evolution of a physical system is represented by its *phase space trajectory*. Of course, the phase space trajectories $x(t)$ are differentiable with respect to t.[2]

We define an *autonomous system* as a system which is *time-invariant*, i.e. the HAMILTON function $H(x, t)$ does not depend explicitly on time t, $H(x, t) \equiv H(x)$. Hence, a physical system is referred to as autonomous if the HAMILTON function $H(x, t)$ of the system obeys

$$\frac{\partial}{\partial t} H(x, t) = 0 \, . \tag{6.25}$$

Thus, the total energy is conserved.

An autonomous system is referred to as *integrable* if it has f independent invariants $I_1, \ldots, I_f$

$$I_j(x) = I_j = \text{const}, \quad j = 1, \ldots, f \, . \tag{6.26}$$

One of these is the energy. Each particular invariant I_j reduces the dimension of the manifold on which the phase space trajectories can propagate. Hence, an integrable system propagates on an f-dimensional subspace of the $2f$-dimensional phase space. We note that a one-dimensional autonomous system is integrable since the conservation of energy delivers the required invariant.

On the other hand, non-integrable systems can show chaotic behavior. In this case the trajectories develop a strong dependence on the initial conditions which makes an analytic calculation of the dynamics extremely difficult. However, since the trajectories can be computed without problems by numeric means, we discuss now how to characterize chaotic behavior on the computer.

For this sake we investigate the dynamics of an autonomous Hamiltonian system starting with one of two initial conditions, namely x_0 and x_0'. Then the system arrives at time t at the phase space points $x(t) = \varphi_t(x_0)$ and $x'(t) = \varphi_t(x_0')$, respectively, as a solution of HAMILTON's equations of motion. Here $\varphi_t(x_0)$ denotes the flow of the system as defined in Sect. 5.4. Since the trajectories in a chaotic system strongly depend on the initial conditions x_0 and x_0' we introduce the separation between the two trajectories $\varphi_t(x_0)$ and $\varphi_t(x_0')$ at time t as $d(t) = |\varphi_t(x_0) - \varphi_t(x_0')|$ where $|\cdot|$ denotes some suitable norm. This length can now, for instance, be used to characterize the *stability* of the trajectory $\varphi_t(x_0)$ [11]. In particular, a solution $\varphi_t(x_0)$ is referred to as stable if

$$\forall \epsilon > 0 \; \exists \delta(\epsilon) > 0 : \forall x_0' : d(0) < \delta \Rightarrow d(t) < \epsilon, \quad \forall t > 0 \, . \tag{6.27}$$

In words: We speak of a stable solution if the trajectory $\varphi_t(x_0')$ which corresponds to the perturbed initial condition x_0' stays within a tube of radius ϵ around the

[2]The symplectic mapping $\varphi_t : x_0 \mapsto x(t)$ from the initial conditions x_0 to the phase space point $x(t)$ at time t is referred to as *Hamiltonian flow* of the system. This was discussed in Sect. 5.4.

unperturbed trajectory $\varphi_t(x_0)$ *for all* $t > 0$. Alternatively, a solution is referred to as asymptotically stable if the distance to adjacent trajectories tends to zero, i.e. $d(t) \to 0$ as $t \to \infty$. Such solutions tend to attract trajectories from their neighborhood and, hence, they are referred to as *attractors*. Finally, a *periodic orbit* is defined as a trajectory for which one can find a time τ such that:

$$\varphi_\tau(x) = x\,, \quad \forall x. \tag{6.28}$$

To find an easy answer to the question whether or not a particular solution of a non-integrable system is stable, the clear, topological method of POINCARÉ maps was introduced. The idea was to reduce the investigation of the complete $2f$-dimensional phase space trajectory $x(t) = \varphi_t(x_0)$ to the investigation of its *intersection* points through a plane Σ which is transverse to the flow of the system. This plane is a subspace of dimension $2f - 1$ and is commonly referred to as POINCARÉ section [3]. The transversality of the POINCARÉ section Σ means that periodic flows intersect this section and never flow parallel to or within it.

Consider a trajectory which is bound to a finite domain, i.e. it does not tend to infinity in any phase space coordinate. In this case it is possible to define the POINCARÉ section in such a way that the trajectory will intersect this section not only once but several times. Thus, a POINCARÉ map is then the mapping of one intersection point P onto the next intersection point P'.

Let us substantiate this idea: we consider the initial condition x_0 for which a trajectory Γ is periodic. We choose the initial time $t = 0$ in such a way that $x_0 \in \Sigma$, where Σ is the POINCARÉ section, Fig. 6.7. We suppose that after a time $\tau(x_0)$ the trajectory intersects this POINCARÉ section again.[3] Since we demanded that the trajectory which started in x_0 is periodic, we deduce that it intersects the POINCARÉ section again at some point $\varphi_{\tau(x_0)}(x_0) = x_0$. We consider now a slightly perturbed initial condition $x' \in U_0(x_0)$, where $U_0(x_0)$ is referred to as the *neighborhood* of x_0. In this case the trajectory will in general not be periodic, and the next intersection point $\varphi_{\tau(x')}(x') \neq x'$. The mapping from one intersection point x' onto the next intersection point $\varphi_{\tau(x')}(x')$ is called the POINCARÉ map $P(x') = \varphi_{\tau(x')}(x')$. We note that the particular point x_0 is a fixed point of this mapping, $P(x_0) = x_0$. Furthermore, we note that if $x' \in U_0(x_0)$ we will have $P(x') \in U_1(x_0)$, where $U_1(x_0)$ is the neighborhood of first return. This is indicated schematically in Fig. 6.7.

[3]Note that we denoted $\tau \equiv \tau(x_0)$ in order to emphasize that the recurrence time τ will depend on the initial condition x_0.

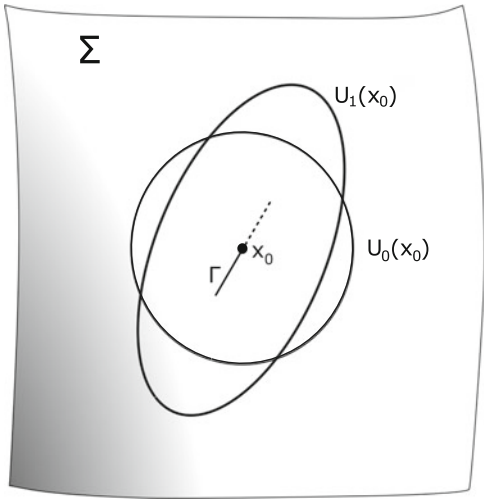

Fig. 6.7 Schematic illustration of the neighborhood $U_0(x_0)$ and the neighborhood of first return $U_1(x_0)$ of a periodic trajectory Γ. The intersection point x_0 of Γ with Σ is a fixed point of this mapping

We utilize now these concepts and analyze the dynamics of the double pendulum. We have four generalized coordinates which, with the help of conservation of energy, are constrained to a three-dimensional manifold within the four-dimensional phase space. Since the investigation of these three-dimensional trajectories is very complex we consider a two-dimensional POINCARÉ section. For instance, the coordinates $[\varphi_1(t), p_1(t)]^T$ can be 'measured' whenever $\varphi_2(t) = 0$ and $p_2 > 0$. Thus, the system's state is registered whenever mass 2 crosses the vertical plane from the left-hand side.

We discuss now some of the most typical scenarios for POINCARÉ plots. (Such a plot represents the POINCARÉ section together with all intersection points of a particular trajectory.) Note that this discussion is, of course, not restricted to the case of the double pendulum. Two different scenarios can be distinguished for integrable systems: (i) the set of intersection points $(\eta_1, \eta_2, \ldots, \eta_N)$ is finite. (ii) In the more general case, the dimension N of the set of intersection points is infinite. In both cases the intersection points form one-dimensional lines which do not have to be connected. Figure 6.8a, b discuss this schematically. However, if the system is non-integrable, a third scenario is possible: chaotic behavior. In this case the intersection points appear to be randomly distributed on the two-dimensional POINCARÉ section and one observes space-filling behavior. This is illustrated schematically in Fig. 6.8c. Whether one observes chaotic behavior or not depends on the choice of the initial conditions.

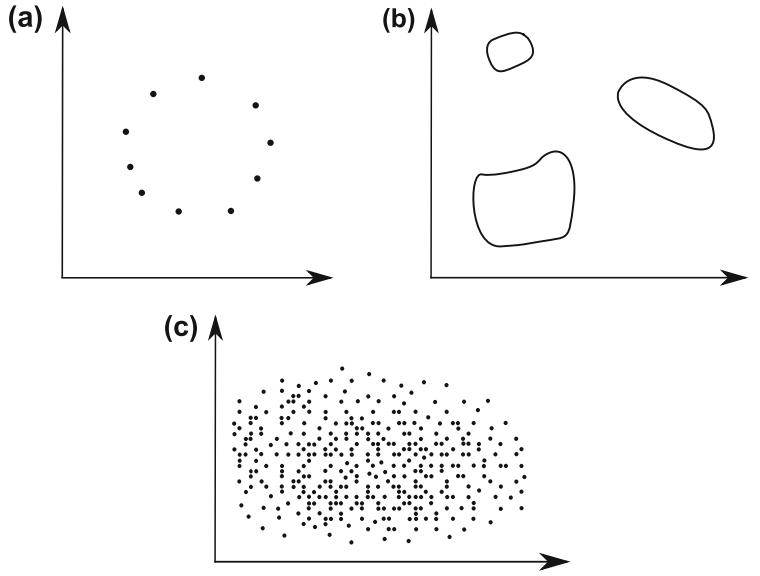

Fig. 6.8 Schematic illustration of the three types of POINCARÉ plots as discussed in the text. **(a)** Finite number of intersection points, **(b)** infinite number of intersection points which, however, form closed lines, **(c)** space-filling and, consequently, chaotic behavior

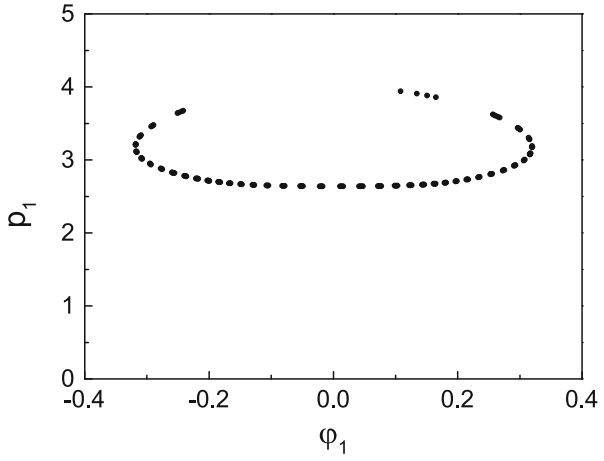

Fig. 6.9 POINCARÉ plot of the double pendulum with initial conditions $\varphi_1(0) = \varphi_2(0) = 0.0$, $p_1(0) = 4.0$ and $p_2(0) = 2.0$. It corresponds to the situation discussed in Fig. 6.2

In Figs. 6.9, 6.10, and 6.11 we present POINCARÉ plots of the double pendulum. The graphs were obtained with help of the method discussed above, i.e. $\varphi_2 = 0$ and $p_2 > 0$. Again, we set $m = \ell = 1$ and $g = 9.8067$. The time step was chosen to be $\Delta t = 0.001$ and we calculated $N = 36 \times 10^4$ time steps. In Figs. 6.9 and 6.10

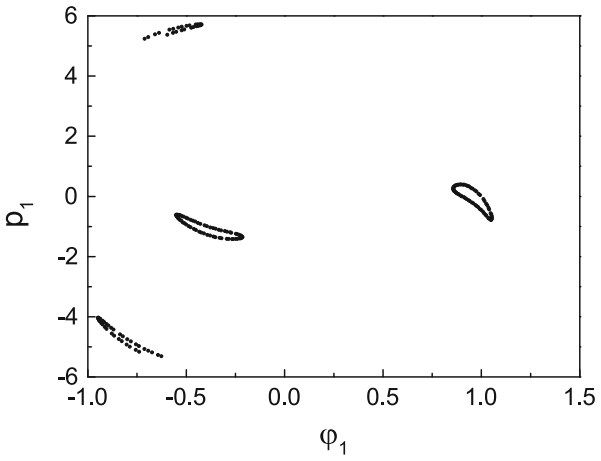

Fig. 6.10 POINCARÉ plot of the double pendulum with initial conditions $\varphi_1(0) = 1.0, \varphi_2(0) = 0.0$, $p_1(0) = 0.0$ and $p_2(0) = 3.0$. It corresponds to the situation discussed in Fig. 6.3

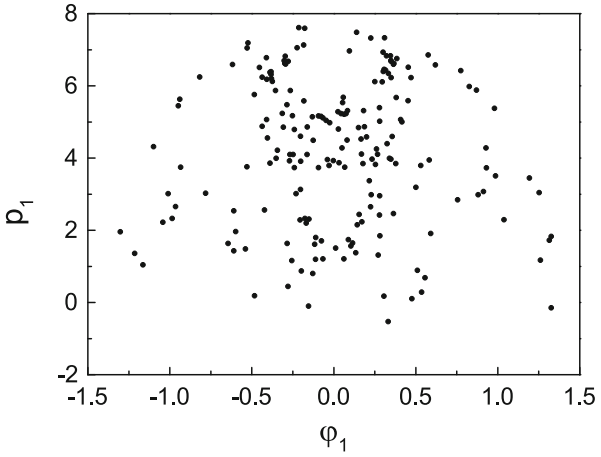

Fig. 6.11 POINCARÉ plot of the double pendulum with initial conditions $\varphi_1(0) = \varphi_2(0) = 0.0$, $p_1(0) = 0.0$ and $p_2(0) = 4.0$. It corresponds to the situation discussed in Fig. 6.4

we observe regular behavior as it was illustrated in Fig. 6.8b. In Fig. 6.11 the points are space filling and, consequently, chaotic behavior is observed in this particular case. Keeping in mind that this particular POINCARÉ plot refers to the initial value problem of Fig. 6.4 we conclude that all problems of this series, i.e. Figs. 6.4, 6.5, and 6.6, are non-integrable and chaotic.

Summary

The dynamics of the double pendulum is described by a system of four ordinary first order differential equations. It is a typical initial value problem and, thus, the methods introduced in Chap. 5 are all candidates to find a numerical solution. Here we concentrated on the explicit RUNGE-KUTTA algorithm *e-RK-4* of Sect. 5.3.

Solutions were studied in detail for several classes of initial conditions. One of the results was that rather small changes of the initial conditions could result in rather strong, chaotic reactions of the outer mass. This triggered the obvious question about the stability of a numerical analysis and of physical dynamics in general. While the stability of numerical methods has already been discussed in Chap. 1 we focused here on the chaotic behavior of Hamiltonian systems. Consequently, a short section on the numerical analysis of chaos was added. It contained the most important concepts and in particular the concept of the stability of a phase space trajectory against variation of initial conditions. Finally, the importance of POINCARÉ plots in recognizing whether a system is integrable or non-integrable was explained. Non-integrable systems can develop chaotic behavior. Thus, POINCARÉ plots are an important tool to study chaos in mechanics.

Problems

1. Verify HAMILTON's equations of motion derived in Sect. 6.1. Implement the *e-RK-4* algorithm discussed in Sects. 5.3 and 6.2 to integrate the equations of motion. Plot the trajectories for various initial conditions. Use the examples illustrated in Sect. 6.2 to check the code.
2. Produce POINCARÉ plots by plotting (φ_1, p_1) whenever $\varphi_2 = 0$ and $p_2 > 0$. The condition $\varphi_2 = 0$ is substituted by $|\varphi_2| < \epsilon$ in the numerically realization. Note that if the points are space filling the dynamics are chaotic, as discussed in Sect. 6.3. Try to find different initial conditions which result in regular behavior and different initial conditions which produce chaotic dynamics.
3. Let $x(t) = [\varphi_1(t), \varphi_2(t), p_1(t), p_2(t)]^T$ and $x'(t) = [\varphi_1'(t), \varphi_2'(t), p_1'(t), p_2'(t)]^T$ be two trajectories which correspond to different initial conditions x_0 and x_0'. In this case the distance between trajectories is defined as

$$d(t) = \sqrt{[\varphi_1(t) - \varphi_1'(t)]^2 + [\varphi_2(t) - \varphi_2'(t)]^2 + [p_1(t) - p_1'(t)]^2 + [p_2(t) - p_2'(t)]^2}.$$

   Plot the distance $d(t)$ as a function of time t for two different initial conditions.
4. Extend the code of the double pendulum of equal mass and equal length to cover the case when the lengths and masses of the individual pendula are different, $\ell_1 \neq \ell_2$ and $m_1 \neq m_2$. What happens? For instance, one can choose a certain initial condition and keep ℓ_1 and ℓ_2 fixed. What is the influence of ℓ_1 and ℓ_2 on the dynamics?
5. Show that the dynamics become integrable in the absence of a gravitational force, i.e. $g = 0$. What are the conserved quantities? How do the POINCARÉ plots look like? Again, try different initial conditions.

References

1. Arnol'd, V.I.: Mathematical Methods of Classical Mechanics, 2nd edn. Graduate Texts in Mathematics, vol. 60. Springer, Berlin/Heidelberg (1989)
2. Fetter, A.L., Walecka, J.D.: Theoretical Mechanics of Particles and Continua. Dover, New York (2004)
3. Scheck, F.: Mechanics, 5th edn. Springer, Berlin/Heidelberg (2010)
4. Goldstein, H., Poole, C., Safko, J.: Classical Mechanics, 3rd edn. Addison-Wesley, Menlo Park (2013)
5. Fließbach, T.: Mechanik, 7th edn. Lehrbuch zur Theoretischen Physik I. Springer, Berlin/Heidelberg (2015)
6. Arnol'd, V.I.: Catastrophe Theory. Springer, Berlin/Heidelberg (1992)
7. McCauley, J.L.: Chaos, Dynamics and Fractals. Cambridge University Press, Cambridge (1994)
8. Devaney, R.L.: An Introduction to Chaotic Dynamical Systems, 2nd edn. Westview, Boulder (2003)
9. Schuster, H.G., Just, W.: Deterministic Chaos, 4th edn. Wiley, New York (2006)
10. Teschl, G.: Ordinary Differential Equations and Dynamical Systems. Graduate Studies in Mathematics, vol. 140. American Mathematical Society, Providence (2012)
11. Lyapunov, A.M.: The General Problem of Stability of Motion. Taylor & Francis, London (1992)